Fractional-order variational numerical methods for tomographic reconstruction of binary images

Maïtine Bergounioux, Erwann Le Pennec, Emmanuel Trélat

Fractional-order variational numerical methods for tomographic reconstruction of binary images

M. Bergounioux E. Le Pennec E. Trélat *

May 17, 2018

Abstract

The aim of this article is to provide and compare several numerical methods for the tomographic reconstruction of blurred and noised binary images, based on one single snapshot taken from an axially symmetric 3D object. This problem is motivated by a physical experiment of the CEA, where a single radiography is taken during the implosion process of some dense such object and is strongly blurred and noised. In a previous article [3] we have provided a refined functional analysis of the Radon operator restricted to axisymmetric functions and proved that it enjoys strong regularity properties in fractional order Hilbert spaces. Based on that theoretical study, we provide here the details of the numerical solving of a minimization problem settled in suitable fractional order Hilbert spaces, using a numerical approximation of the fractional Laplacian and some adapted Newton-like methods. The resulting procedure happens to be very efficient, both for the execution time and for the quality of the reconstruction. We compare this approach with two other numerical approaches: the first one uses the Fourier transform, and the second uses a wavelet reconstruction sofware.

Keywords: tomographic reconstruction, Radon operator, fractional Laplacian, minimization, Fourier transform, wavelets.

1 Introduction

The goal of this article is to provide an efficient numerical method for the tomographic reconstruction of blurred and noised binary images, based on one single radiography. This problem is motivated by a physical experiment led at the CEA[1] consisting of reconstructing the shape of an axially symmetric 3D object at some precise moment of its implosion, using one single X-ray radiography. Due to the experimental conditions, the snapshot is strongly noised and blurred. Moreover it is assumed that the object is made of one homogeneous

*Université d'Orléans, UFR Sciences, Math., Labo. MAPMO, UMR 6628, Route de Chartres, BP 6759, 45067 Orléans cedex 2, France. E-mail: maitine.bergounioux@univ-orleans.fr, emmanuel.trelat@univ-orleans.fr,erwan.le-pennec@polytechnique.edu

[1]Commissariat à l'Energie Atomique, Bruyères-le-Châtel, France

material and of some holes, thus is considered as being binary. It must be noted that there exist few results or methods for such tomographic reconstruction problems.

The modelization has been done in details in [1], and we next briefly recall how the problem can be expressed in terms of the Radon transform. We assume that the object is quite small, and is far from the X-ray source, so that X-rays can be considered parallel and orthogonal to the symmetry axis of the object. In these conditions, taking Cartesian coordinates (y, z) on the radiograph, the Radon transform of the object is defined by the projection operator

$$(H_0 u)(y, z) = 2 \int_{|y|}^{+\infty} u(r, z) \frac{r}{\sqrt{r^2 - y^2}} dr, \tag{1.1}$$

for all $y, z \in \mathbb{R}$, where the function u (with compact support) denotes the density of the object and is expressed in cylindrical coordinates (r, z), where the z-axis corresponds to the (vertical) symmetry axis of the object. It is understood that, since the object under consideration is compact, the integral above is actually on a finite interval. To be more precise, we consider density functions that are bounded variation functions defined on $\mathbb{R}^+ \times \mathbb{R}$, having a compact support contained in the subset $\Omega = [0, a) \times (-a, a)$ of $\mathbb{R}^2$, where $a > 0$ is fixed, and taking their values in the binary set $\{0, 1\}$. In particular, the upper bound of the integral in (1.1) can be set to a, and for every such density function u, the function $H_0 u$ is of compact support contained in $\Omega_1 = (-a, a)^2$.

As mentioned previously, due to the experimental conditions the available (single) radiography is strongly blurred and noised, and hence the data from the snapshot at our disposal are of the form

$$v_d = B H_0 u + \tau, \tag{1.2}$$

where B is a linear operator modeling the blur[2], and τ is a noise[3]. In the sequel, we set $H = B H_0$.

In practice, given observed data v_d, it is our aim to provide a reconstruction u of the density of the object which would be as accurate as possible. As is well known, this inverse problem is very ill-posed, due to the bad-conditioning of the Radon operator H_0. Applying (formally) the inverse of H_0 to v_d causes significant errors and can only provide a low-quality reconstruction of the object.

To deal with this ill-posed problem, we have first proposed in [1] a variational approach consisting of minimizing

$$\frac{1}{2} \|Hu - v_d\|^2_{L^2(\Omega_1)} + \alpha \Phi(u) \tag{1.3}$$

over all possible bounded variation functions defined on Ω and satisfying $u(x) \in \{0, 1\}$ almost everywhere on Ω. Here, $\alpha > 0$ is a fixed parameter to be chosen, and $\Phi(u)$ denotes the total variation of the bounded variation function u. This minimization procedure leads to a method of tomographic reconstruction in our problem.

To be more precise with the mathematical setting, recall that $BV(\Omega)$ is the space of bounded variation functions, that are functions $u \in L^1(\Omega)$ whose distributional gradient

[2] Usually, B is the convolution with a positive symmetric kernel K with compact support and such that $\int K d\mu = 1$

[3] Usually, an additive Gaussian white noise of zero mean

Du is a finite vector Radon measure, satisfying

$$\int_\Omega u \operatorname{div} \varphi \, dx = -\langle Du, \varphi \rangle = -\int_\Omega \varphi \cdot d(Du) = -\int_\Omega \varphi \cdot \sigma_u \, d|Du|,$$

for every $\varphi \in \mathcal{C}^1_c(\Omega, \mathbb{R}^2)$, where $\mathcal{C}^1_c(\Omega, \mathbb{R}^2)$ is the space of continuously differentiable vector functions of compact support contained in Ω, and where $\sigma_u : \Omega \to \mathbb{R}^2$ is a $|Du|$-measurable function satisfying $|\sigma_u| = 1$ almost everywhere on Ω. Then, recall that the total variation of $u \in BV(\Omega)$ is defined by

$$\Phi(u) = \sup \left\{ \int_\Omega u(x) \operatorname{div} \varphi(x) \, dx \;\middle|\; \varphi \in \mathcal{C}^1_c(\Omega, \mathbb{R}^2), \;\; \|\varphi\|_{L^\infty} \leqslant 1 \right\} = \int_\Omega |Du| = |Du|(\Omega).$$

Endowed with the norm $\|u\|_{BV} = \|u\|_{L^1} + \Phi(u)$, the space $BV(\Omega)$ is a Banach space.

Note that it has been shown in [1] that H_0 extends to a linear continuous operator from $L^2(\Omega)$ to $L^2(\Omega_1)$, and hence minimizing (1.3) makes sense, at least provided that $v_d \in L^2(\Omega_1)$. From the practical point of view, the nonconvex binarity constraint $u(x) \in \{0, 1\}$ a.e. is hard to tackle numerically, and in [1] a penalization procedure is proposed, consisting in introducing a new parameter $\varepsilon > 0$, and minimizing rather

$$\frac{1}{2}\|Hu - v_d\|^2_{L^2(\Omega_1)} + \frac{1}{2\varepsilon}\|u - u^2\|^2_{L^2(\Omega)} + \alpha\Phi(u) \tag{1.4}$$

over all functions $u \in BV(\Omega)$. This leads to an interesting numerical method that however does not provide very satisfactory results. In [3] we made a refined study of the intrinsic regularity properties of the projection operator, which leads to reconsider the above minimization procedure with a more adapted norm. It is the object of that paper to show that, combining this theoretical study with a careful numerical implementation leads to spectacular numerical improvements. Let us first recall, in the next section, the main results of [3].

2 Fractional variational approach

2.1 Refined functional properties of the Radon operator

Regularity properties of the Radon transform and their applications to tomography have been widely investigated in the literature (see e.g. [1, 2, 6, 7, 8, 9, 11]), but are generally stated in the spaces L^p. As mentioned above, it has been shown in [1] that the use of such norms indeed provides acceptable reconstruction processes, but they will happen to be largely improved by taking into account stronger regularity features. A refined functional analysis of the Radon projection operator H_0 defined by (1.1) was led in [3], stating that it enjoys strong regularity properties in fractional order Hilbert spaces. We next recall these results. Denote by

$$X = L^2(-a, a; BV_0(0, a)) \tag{2.1}$$

the set of all functions $u \in L^2(\Omega)$ such that the function $(z, r) \mapsto u(r, z)$ belongs to $L^2(-a, a; BV_0(0, a))$, where $BV_0(0, a)$ is the closed subset of the set of functions $f \in$

$BV(0,a)$ vanishing at a. The total variation, which is a semi-norm, is a norm on $BV_0(0,a)$. Hence the space X is a closed subspace of the Banach space $L^2(-a,a;BV(0,a))$, and can be endowed with the norm

$$\|u\|_X = \left(\int_{-a}^{a} \left(|Du_z|(0,a)\right)^2 \, dz\right)^{1/2} = \left(\int_{-a}^{a} \left(\varphi(u_z)\right)^2 \, dz\right)^{1/2}, \tag{2.2}$$

where the notation u_z stands for the function $r \mapsto u_z(r) = u(r,z)$, and where the notation $\varphi(f)$ is used to denote the total variation of a function $f \in BV(0,a)$.

For every $s \in (0,1)$, the fractional order Hilbert space $H^s(-a,a)$ is defined as the space of all functions $f \in L^2(-a,a)$ such that

$$\int_{-a}^{a}\int_{-a}^{a} \frac{|f(x)-f(y)|^2}{|x-y|^{1+2s}} dx\, dy \ < +\infty,$$

endowed with the norm

$$\|f\|_{H^s(-a,a)} = \left(\|f\|^2_{L^2(-a,a)} + \int_{-a}^{a}\int_{-a}^{a} \frac{|f(x)-f(y)|^2}{|x-y|^{1+2s}} dx\, dy\right)^{1/2}.$$

It is possible to define the Hilbert space $H^s(-a,a)$ in other equivalent ways, in particular with the Fourier transform or with the fractional Laplacian operator (see [3] for a survey of equivalent definitions).

The space $H^s_0(-a,a)$ is defined as the closure in $H^s(-a,a)$ of the set of all smooth functions having a compact support contained in $(-a,a)$. Note that, for $s \in [0,1/2]$, there holds $H^s_0(-a,a) = H^s(-a,a)$. The Lions-Magenes space $H^{1/2}_{00}(-a,a)$ is the subset of functions $f \in H^{1/2}(-a,a)$ such that $\rho^{-1/2} f \in L^2(-a,a)$, where the function ρ is defined on $(-a,a)$ by $\rho(y) = a - |y|$.

For every $s \in [0,1) \setminus \{1/2\}$, denote by

$$Y_s = L^2(-a,a;H^s_0(-a,a)) \tag{2.3}$$

the set of all functions $v \in L^2(\Omega_1)$ such that the function $(z,y) \mapsto v(y,z)$ belongs to $L^2(-a,a;H^s_0(-a,a))$. It is a closed subspace of $L^2(-a,a;H^s(-a,a))$, and, endowed with the norm

$$\|v\|_{Y_s} = \left(\int_{-a}^{a} \|v(\cdot,z)\|^2_{H^s(-a,a)} \, dz\right)^{1/2}, \tag{2.4}$$

Y_s is a Hilbert space. For $s = 1/2$, define, similarly, the Hilbert space

$$Y_{1/2} = L^2(-a,a;H^{1/2}_{00}(-a,a)). \tag{2.5}$$

Theorem 1 ([3]). *For every $s \in [0,1)$, the operator H_0 is linear and continuous from X into Y_s.*

Note that this result holds as well for the blurred projection operator $H = BH_0 = K \star H_0$. Note also that other regularity properties have been derived in [3], but the previous theorem is particularly useful in view of taking benefit of the Hilbert structure.

2.2 Minimization problem in fractional Sobolev spaces

Based on the functional properties stated in Theorem 1, we have proposed in [3] to consider the following minimization problem. Let $s \in [0,1)$, let α and β be nonnegative real numbers, and let $\varepsilon > 0$. The projected image v_d (observed data) is assumed to belong to Y_s. Consider the problem of minimizing

$$F^s_{\alpha,\beta,\varepsilon}(u) = \frac{1}{2}\|Hu - v_d\|^2_{Y_s} + \alpha\Phi(u) + \frac{\beta}{2}\|u\|^2_X + \frac{1}{2\varepsilon}\|u - u^2\|^2_{L^2(\Omega)} \tag{2.6}$$

among all functions $u \in X$ where $\mathcal{X} = X$ whenever $\alpha = 0$, and $\mathcal{X} = BV(\Omega) \cap X$ whenever $\alpha > 0$.

Remark 1. In fact the minimimu of $F^s_{\alpha,\beta,\varepsilon}$ shoud be found among all functions $u \in \mathcal{B}_\eta$ where $\eta > 0$ and

$$\mathcal{B}_\eta := \{\, u \in \mathcal{X} \mid \beta\|u\|_X + \|u\|_\infty \leq \eta \,\}.$$

Indeed, becasue of the lack of coercivity of the functional we need a boundness constraint to prove existence result within the infinite dimensional framework. However, we are allowed to choose any (large enough) η and the solution to the orginal (non penalized) problem exists without any additional condition. Therefore, from the pratical point of view, this constraint will be inactive and we do not take it into account for numerical purpose.

The parameter α is the weight of the total variation. If $\alpha > 0$ then this term yields a regularization term used in a standard way in image processing. Note here that we introduce an alternative to this usual regularization, with the term $\|u\|^2_X$, weighted with β. Note that in our method it is required that $\alpha + \beta > 0$, that is, if $\alpha = 0$ then β must be chosen positive, and conversely. Note that $F^s_{\alpha,\beta,\varepsilon}$ is not differentiable because of these terms.

The parameter $\varepsilon > 0$ is a penalization parameter. The limit case $\varepsilon = 0$ corresponds to the binarity constraint $u(r,z) \in \{0,1\}$ a.e. on Ω, and for this limit case it has been proved in [3] that the associated minimization problem has at least one solution. It has been proved as well that the minimization problem (2.6) is well defined and has at least one solution whenever $\varepsilon > 0$, and this family of optimization problems parameterized by ε enjoys a nice Γ-convergence property to the limit case.

First-order necessary conditions for optimality of (2.6) have been derived in [3] in the form of an optimality system, as explained next. Although $F^s_{\alpha,\beta,\varepsilon}$ is not differentiable, the functional defined by

$$G^s(u) = \frac{1}{2}\|Hu - v_d\|^2_{Y_s} \tag{2.7}$$

is differentiable, and in what follows we denote by $\nabla G^s(u)$ its gradient for the pivot space L^2. It can be computed in several ways, in particular using a fractional Laplacian or using the Fourier transform. This will lead to different numerical implementation methods. The functional $u \mapsto \frac{1}{2\varepsilon}\|u - u^2\|^2_{L^2(\Omega)}$ is differentiable as well, and its gradient for the pivot space L^2 is

$$q_\varepsilon(u) = \frac{(u - u^2)(1 - 2u)}{\varepsilon}. \tag{2.8}$$

Recall that $X = L^2(-a,a;BV_0(0,a))$, and thus $X' = L^2(-a,a;(BV_0(0,a))')$. For every $\lambda \in X'$, viewed as function of $z \in (-a,a)$ of class L^2 with values in $(BV_0(0,a))'$, denote $\lambda_z = \lambda(z) \in (BV_0(0,a))'$, for almost every $z \in (-a,a)$. The duality product between X and X' is defined by

$$\langle \lambda, v \rangle_{X',X} = \int_{-a}^{a} \langle \lambda_z, v_z \rangle_{BV_0',BV_0} \, dz,$$

for every $\lambda \in X'$ and every $v \in X$. Finally, recall that the notation $\varphi(f)$ is used to denote the total variation of a function $f \in BV(0,a)$.

Theorem 2 ([3]). *Let u be a minimizer of (2.6) with the constraint $u \in \mathcal{B}_\eta$. Then there exist $\rho \in (\mathcal{M}(\Omega)^2)'$, $\mu = -div\ \rho$, and $\lambda \in X'$, such that*

$$\nabla G^s(u) + q_\varepsilon(u) + \alpha\mu + \beta\lambda = 0, \tag{2.9}$$

$$\mu \in \partial\Phi(u), \tag{2.10}$$

and

$$\lambda_z \in \varphi(u_z)\, \partial\varphi(u_z), \tag{2.11}$$

for almost every $z \in (-a,a)$.

We use an iterative fixed-point method to compute the solution to (2.9)-(2.10)-(2.11).

3 Numerical implementation of the fractional variational approach

3.1 The general algorithm

In this section we explain how to carry out the numerical implementation of the optimality necessary conditions stated in Theorem 2. Notice that the method will depend on the four parameters s, α, β, and ε. Their respective role will be explained and discussed further. **These parameters being fixed,** we propose the following iterative algorithm.

Algorithm 1

Initialization : Initialization: $n = 0$, choose $u^0 = H_0^{-1} v_d$.
N_∞ maximum number of iterations.
Iterations :
for $0 \leqslant n \leqslant N_\infty$ **do**
(a) Determine $\mu^n \in \partial\Phi(u^n)$.
(b) Determine $\lambda_z^n \in \varphi(u_z^n)\, \partial\varphi(u_z^n)$, for every discretized value of $z \in (-a,a)$.
(c) Make p fixed-point-like iterations for the solving of

$$\nabla G^s(u^{n+1}) + q_\varepsilon(u^{n+1}) + \alpha\mu^n + \beta\lambda^n = 0.$$

(d) Stopping criterion: $|F^s_{\alpha,\beta,\varepsilon}(u^{n+1}) - F^s_{\alpha,\beta,\varepsilon}(u^n)|$ small enough
end for

We next discuss the discretization process, the steps of that algorithm, and the different implementation choices that can be done.

Discretization process. As usually, the discretized image is represented by a $N \times N$ array. Due to the symmetry, it suffices to deal with half an image, of size $N \times N/2$. Denote $X = \mathbb{R}^{N \times N}$ and $Y = X \times X$, endowed with the usual scalar product. For $u \in X$, the approximation of the Radon measure Du is identified with a vector of Y of coordinates $(Du)_{i,j} = ((Du)^1_{i,j}, (Du)^2_{i,j})$ defined by

$$(Du)^1_{i,j} = \begin{cases} u_{i+1,j} - u_{i,j} & \text{if} \quad i < N, \\ 0 & \text{if} \quad i = N, \end{cases} \qquad (Du)^2_{i,j} = \begin{cases} u_{1,j+1} - u_{i,j} & \text{if} \quad j < N, \\ 0 & \text{if} \quad j = N, \end{cases}$$

and the approximation of total variation is

$$\Phi(u) = \sum_{1 \leqslant i,j \leqslant N} \sqrt{((Du)^1_{i,j})^2 + ((Du)^2_{i,j})^2}.$$

The divergence operator is discretized through

$$(\text{div } p)_{i,j} = \begin{cases} p^1_{i,j} - p^1_{i-1,j} & \text{if} \quad 1 < i < N \\ p^1_{i,j} & \text{if} \quad i = 1 \\ -p^1_{i-1,j} & \text{if} \quad i = N \end{cases} + \begin{cases} p^2_{i,j} - p^2_{i,j-1} & \text{if} \quad 1 < j < N \\ p^2_{i,j} & \text{if} \quad j = 1 \\ -p^2_{i,j-1} & \text{if} \quad j = N \end{cases}$$

Initialization. It is natural to initialize the algorithm with $u^0 = H_0^{-1} v_d$, that is, by applying the inverse of the (discretized) Radon transform to the observed data. As mentioned previously, the resulting image u^0 cannot be expected to be a nice reconstruction of the object (see also numerical simulations further), since it is far too much noised and blurred, however is the most natural initial point of our iterative procedure. A random initializations could do not lead to a satisfying reconstruction since, in some sense, our algorithm acts as denoising and deblurring.

Subdifferential of the total variation. The choice of $\mu \in \partial\Phi(u)$ or $\lambda_z \in \varphi(u_z)\, \partial\varphi(u_z)$ in (2.10)-(2.11) follows Chambolle's method (see [4]). We briefly recall the idea for the construction of $\mu \in \partial\Phi(u)$ in the discretized setting. Recall that the Fenchel-Legendre conjugate function Φ^* of Φ is the indicatrix function $1_{\mathcal{K}_2}$ of

$$\mathcal{K}_2 = \{\text{div } g \mid g \in Y,\ (g^1_{i,j})^2 + (g^2_{i,j})^2 \leqslant 1,\ \forall i, j\}.$$

Moreover,

$$\mu \in \partial\Phi(u) \Leftrightarrow u \in \partial 1_{\mathcal{K}_2}(\mu) \Leftrightarrow \mu = \Pi_{\mathcal{K}_2}(\mu + u)$$

where $\Pi_{\mathcal{K}_2}$ denotes the orthogonal projection on $\mathcal{K}_2$. Therefore, μ can be computed with the successive approximation process $\mu_k = \Pi_{\mathcal{K}_2}(\mu_{k-1} + u)$ or with a semi-smooth Newton method.

Similarly, for every discretized value of $z \in (-a, a)$., we compute $\lambda_z \in \varphi(u_z)\,\partial\varphi(u_z)$ as

$$\lambda_z = \varphi(u_z)\tilde{\lambda}_z \text{ with } \tilde{\lambda}_z = \Pi_{\mathcal{K}_1}(\tilde{\lambda}_z + u_z)$$

and

$$\mathcal{K}_1 = \{g' \ | g \in \mathbb{R}^N \times \mathbb{R}^N,\ (g_i^1)^2 + (g_i^2)^2 \leqslant 1,\ \forall i\}.$$

Therefore, $\tilde{\lambda}_z$ can also be computed with the successive approximation process $(\tilde{\lambda}_z)_k = \Pi_{\mathcal{K}_1}((\tilde{\lambda}_z)_{k-1} + u_z)$.

The projected element $\bar{v} := \Pi_{\mathcal{K}_i}(v) = \text{div}\ \bar{p}$ where $\bar{p} = \text{argmin}\ \{\ \| \text{ div } (p) - v\|_X^2 \mid |p_{i,j}| \leq 1,\ i, j = 1, \cdots, N\ \}$, may be computed using the point-fixed algorithm of Chambolle [4] or a Nesterov-type algorithm described in [12, 14]. The second one is faster than the first one. However, we have noticed that very few iterations were necessary to make the (global) algorithm converge (practically 1 or 2) and the two methods have the same behavior. In addition we have an estimate of the convergence rate of the Nesterov-type algorithm. More precisely, if v_k denotes the k^{th} iterate then

$$0 \leq \ \|v_k - v\|_X^2 - \ \|\bar{v} - v\|_X^2 \leq \frac{C}{(k+1)(k+2)}\ , \tag{3.1}$$

where C is a generic constant.

Fixed-point-like iterations. In order to solve the third step of the iterative loop, we propose to implement a certain number of steps of a fixed-point-like iteration solving, as follows. Given μ^n and λ^n, define $f^n(u) = \nabla G^s(u) + q_\varepsilon(u) + \alpha\mu^n + \beta\lambda^n$. The aim is to estimate u^{n+1} by solving the implicit nonlinear system $f^n(u) = 0$. This is equivalent to seeking u such that

$$u - M^n f^n(u) = u, \tag{3.2}$$

where M^n is a square (preconditioning) matrix to be chosen. We propose here to implement p steps of such a fixed-point procedure initialized at u^n, and the resulting solution is defined to be u^{n+1}. In practice, it happens to be sufficient to take $p = 1$, that is, we implement only one step of this fixed-point procedure.

A standard choice of preconditioner is $M^n = \gamma\,\text{Id}$, with $\gamma > 0$ small enough. This is however not the choice we make. Note that one recovers the classical Newton method whenever one chooses, at each step of the iteration, the matrix M^n to be the inverse of the differential of f^n at the current point. The classical Newton methods is a priori not well adapted here. Indeed, on the one part the discretization of the Radon transform is ill-conditioned, and hence the Hessian of G^s will be ill-conditioned as well, for every possible choice of the discretization of G^s (see further for different ways of computing the gradient of G^s). On the other part, the derivative of the function q_ε defined by (2.8), seen as a function of one scalar variable, is $q_\varepsilon(t) = \frac{1}{\varepsilon}(2t-1)(t^2-t)$, and has three zeros: 0, 0.5, and 1. The classical Newton method for determining the zeros of that scalar function is written as

$$t_{k+1} = t_k - \frac{q_\varepsilon(t_k)}{q'_\varepsilon(t_k)}.$$

However the three zeros are attractive (see Figure 3.1), and in particular the attractive zero $t = 0.5$ should be avoided. Although this analysis is done in dimension 1, when transposed to imaging, a pixel coded with 0.5 is grey, exactly between 0 (black) and 1 (white), but our image is binary and this situation must be avoided. A very simple way, that we can explain in dimension 1, is to modify the classical Newton method so as to make the zero $t = 0.5$ repulsive. Due to the specific expression of the function $q_\varepsilon(\cdot)$, we propose to modify the classical Newton method as follows:

$$t_{k+1} = t_k - 2\frac{q_\varepsilon(t_k)}{|q'_\varepsilon(t_k)|}. \tag{3.3}$$

Let us justify this modification. Define Q_ε the primitive function of q_ε that vanishes at $t = 0$. Then we look for the minima of Q_ε on $[0, 1]$. A descent method with optimal step α_k gives

$$t_{k+1} = t_k - \alpha_k q_\varepsilon(t_k);$$

a classical second order exansion gives

$$Q_\varepsilon(t_{k+1}) - Q_\varepsilon(t_k) = -\alpha_k(q_\varepsilon(t_k))^2 + \frac{\alpha_k^2}{2}(q_\varepsilon(t_k))^2 q'_\varepsilon(t_k) + \circ((t_{k+1} - t_k)^2)\ .$$

The first order analysis gives $\alpha_k > 0$ to let the functional decrease to a local minimum (here 0 or 1). Looking for a second order scheme gives

$$-\alpha_k(q_\varepsilon(t_k))^2 + \frac{\alpha_k^2}{2}(q_\varepsilon(t_k))^2 q'_\varepsilon(t_k) = 0,$$

that is $\alpha_k q'_\varepsilon(t_k) = 2$ which is equivalent to $\alpha_k = 2/|q'_\varepsilon(t_k)|$ since $\alpha_k > 0$.

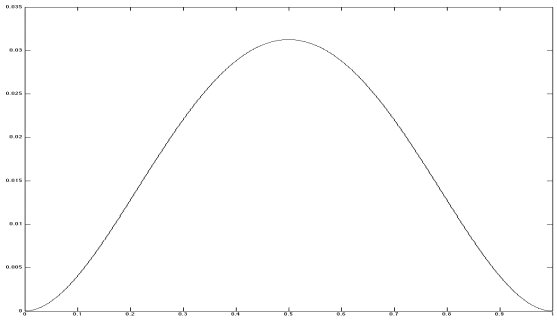

Figure 3.1: Graph of the primitive Q_ε of q_ε: $t \mapsto Q_\varepsilon(t)$

It is then obvious that, on this particular one-dimensional problem, this method is globally convergent, whatever the initialization t_0 may be (except for three particular values). More precisely, for every $t_0 < 1/2$ such that $t_0 \neq \frac{1}{2} - \frac{1}{2\sqrt{3}}$, the iterative sequence (3.3) initialized at t_0 converges to 0, and for every $t_0 > 1/2$ such that $t_0 \neq \frac{1}{2} + \frac{1}{2\sqrt{3}}$, the

iterative sequence (3.3) initialized at t_0 converges to 1. The two particular values $\frac{1}{2} \pm \frac{1}{2\sqrt{3}}$ correspond to the local extrema of the function $q_\varepsilon(\cdot)$, and actually, numerically they even do not cause the divergence of the above method. Indeed, due to the change of sign in (3.3), and for instance in the case $t_0 = \frac{1}{2} + \frac{1}{2\sqrt{3}}$, then numerically t_1 is set to a very large value, and then the next iterates will converge to 1, as expected.

We propose here to transpose this very simple idea to choose an adequate preconditioning matrix M^n for the solving of (3.2). As explained previously, since it suffices to work with half an image, u^n is a matrix of size $N \times N/2$. Then, the matrix $q'_\varepsilon(u^n)$ is as well of size $N \times N/2$, the lines of which are denoted by $L_1(u^n), \ldots, L_N(u^n)$. Then, guided by our one-dimensional analysis, we propose to consider as a matrix M^n, the diagonal $N \times N$-matrix having as diagonal i^{th}-coefficient the scalar $1/\|L_i(u^n)\|$ (using the Euclidean norm). Other choices are of course possible, but this specific choice happens to be the most relevant for our numerical simulations.

We are not able to provide a global convergence rate for Algorithm (3.1). However, the partial computations involve second order schemes and point fixed methods with projections. Therefore, we expect a linear convergence rate.

The previous analysis has been done with fixed parameters. In addition, we may give error estimates for the computed solution with respect to ε and α and/or β as well. For sake of simplicity we set $\beta = 0$. Indeed, we have noticed very small influence of β (see next section). Following [10], we introduce the $\mathcal{R}$-minimizing solution of the problem as

$$u^\dagger := \text{ argmin}\{\mathcal{R}(u), Hu = u_d \},$$

where $\mathcal{R}(u) := \Phi(u) + \|u - u^2\|^2_{L^2(\Omega)}$. As H is surjective, equation $Hu = u_d$ has at least a solution and such a $\mathcal{R}$-minimizer exists. Following Remark 4.5 of [10] and considering that the appropriate assumptions are satisfied, we get

$$\|Hu_\alpha - u_d\|_{Y_s} \leq C\alpha \text{ and } D_{\xi^*}(u_\alpha, u^\dagger) \leq C\alpha \ ,$$

where C is a generic constant, u_α is a minimizer of $F^s_{\alpha,0,1/\alpha}$, $\xi^* \in \partial\mathcal{R}(u^\dagger)$ and $D_{\xi^*}(u_\alpha, u^\dagger)$ is the Bregman-distance :

$$D_{\xi^*}(u_\alpha, u^\dagger) = \mathcal{R}(u_\alpha) - \mathcal{R}(u^\dagger) - < \xi^*, u_\alpha - u^\dagger > \ .$$

3.2 Computation of the fractional derivative ∇G^s

It remains to explain how to compute a good approximation of the gradient ∇G^s. This is the most important issue of our algorithm, in the sense that all previous issues discussed above can be modified but variants lead to quite similar results (both in quality and execution time), whereas the choice of the numerical computation of ∇G^s leads to significant differences. Recall that the functional G^s defined by (2.7) is the square of the norm of the fractional-order Hilbert space Y_s defined by (2.3). We next propose two numerical approaches to estimate such a norm and ∇G^s. The first one uses the Fourier transform and the second one uses an approximation of the fractional Laplacian. Whereas the first one may be expected to be more exact, actually the second one happens to be more relevant for the numerical simulations.

3.2.1 Using the Fourier transform

In this section, we compute ∇G^s using the Fourier transform. First of all, observe that, for every $s \in [0,1)$, for every $u \in Y_s$, the function $Hu - v_d$ can be extended by 0 to a function of $L^2(-a,a;H^s(\mathbb{R}))$, and its norm can be computed in terms of Fourier transform, by

$$\begin{aligned} G^s(u) &= \frac{1}{2}\int_{-a}^{a}\int_{\mathbb{R}} |\mathcal{F}_y(Hu - v_d)(\xi,z)|^2(1+\xi^2)^s \, d\xi \, dz \\ &= \frac{1}{2}\|\mathcal{F}_y(Hu - v_d)\|^2_{L^2(\omega_s)}, \end{aligned}$$

where $L^2(\omega_s)$ denotes the weighted Hilbertian space of all complex valued functions f defined on $\mathbb{R}\times(-a,a)$ such that $\int_{\mathbb{R}\times(-a,a)} |f(\xi,z)|^2\omega_s(\xi)\,d\xi\,dz < +\infty$, where $\omega_s(\xi) = (1+\xi^2)^s$. Setting $w_d = H^{-1}(v_d)$, it follows that

$$\nabla G^s(u) = (\mathcal{F}_y H)^* \omega_s (\mathcal{F}_y H)(u - w_d), \tag{3.4}$$

with L^2 as a pivot space. Moreover, in order to make this expression more explicit, the Fourier transform of the blurred projection operator H can be computed as follows (see [3]). The notation $\tilde{v}$ stands for the extension by 0 to $\mathbb{R}^2$ of any function v. Here it is assumed that the blur is modeled by a linear operator B writing as a convolution with a positive symmetric kernel K (in practice, a Gaussian kernel) with compact support.

Lemma 1. *The Fourier transform of the blurred projection operator $H = BH_0$ with respect to the first variable is*

$$(\mathcal{F}_y B\widetilde{H_0 u})(\xi,z) = (\mathcal{F}_y K)(\xi,\cdot) \star_2 (\mathcal{F}_y \widetilde{H_0 u})(\xi,\cdot)(z), \tag{3.5}$$

for every $u \in L^1(\Omega)$, every $\xi \in \mathbb{R}$ and almost every $z \in (-a,a)$, where the notation $\star_2$ stands for the convolution product with respect to the second variable. Its adjoint (with L^2 as a pivot space) is

$$((\mathcal{F}_y B\widetilde{H_0}^* v)(r,z) = (\mathcal{F}_y \widetilde{H_0})^*(\mathcal{F}_y g \star_2 v)(r,z), \tag{3.6}$$

for every $v \in L^1(\mathbb{R}^2)$, every $r \in [0,a)$ and almost every $z \in (-a,a)$.

3.2.2 Using the fractional Laplacian

In this section, we compute ∇G^s using the fractional Laplacian. By definition, there holds

$$G^s(u) = \frac{1}{2}\int_{-a}^{a} \|(Hu - v_d)(\cdot,z)\|^2_{H_0^s(-a,a)} dz,$$

for every $u \in Y_s$, and every $s \in [0,1)\setminus\{1/2\}$. For $s = 1/2$, $H_0^s(-a,a)$ is replaced with the Lions-Magenes space $H_{00}^{1/2}(-a,a)$. This norm can actually be expressed in an equivalent way using the fractional Laplacian operator, as follows (see [3] for the proofs). For every $f \in H_0^s(-a,a)$ whenever $s \in [0,1)\setminus\{1/2\}$, or $f \in H_{00}^{1/2}(-a,a)$ whenever $s = 1/2$, the

square of the norm of f within these spaces is equivalent to $\|f\|^2_{L^2(U)} + \|(-\Delta)^{s/2} f\|^2_{L^2(\mathbb{R}^n)}$, where f is extended by 0 outside $(-a, a)$ (notice that $(-\Delta)^{s/2} f$ is not of compact support[4]). Here, $(-\Delta)^\alpha$ denotes the fractional Laplacian operator on $\mathbb{R}^n$, defined, using the Fourier transform $\mathcal{F}f$ of f, by $(-\Delta)^\alpha f = \mathcal{F}^{-1}(|\xi|^{2\alpha}\mathcal{F}f)$. It follows that

$$\nabla G^s(u) = H^* R_{\Omega_1}(\mathrm{id} + (-\Delta)^s)(\widetilde{Hu} - \widetilde{v_d}), \tag{3.7}$$

with L^2 as a pivot space, where $\widetilde{Hu} - \widetilde{v_d}$ is the extension of $Hu - v_d$ by 0 outside $(-a, a)$, and R_{Ω_1} is the restriction to Ω_1.

It is very simple to approximate the operator $(-\Delta)^s$. To this aim, consider any usual approximation of the operator $-\Delta$, typically, the tridiagonal matrix

$$N^2 \begin{pmatrix} 2 & -1 & 0 & \cdots & 0 \\ -1 & 2 & -1 & & \vdots \\ 0 & -1 & 2 & \ddots & 0 \\ \vdots & & \ddots & \ddots & -1 \\ 0 & \cdots & 0 & -1 & 2 \end{pmatrix}. \tag{3.8}$$

Since it is a symmetric positive definite matrix, its fractional powers can be computed in many ways, for instance it is straightforward by considering its singular value decomposition (SVD). Note that this computation is done a priori and thus does not slow down the execution of the algorithm. There are some other ways to approximate the Laplacian operator, using higher-order centered schemes, but these variants do not lead to significant differences in the numerical simulations.

3.3 Numerical results

We present hereafter several numerical results. Our working example, drawn on Figure 3.2, represents a synthetic object containing all standard difficulties: several disconnected holes; a small hole located on the symmetry axis (where details are expected to be difficult to recover because the noise variance is maximal around the symmetry axis after reconstruction); smaller details on the boundary of the top hole, serving as a test for lower bound detection. Figure 3.2 (a) represents the shape of an object made of concentric shells of homogeneous materials surrounding a ball of another homogeneous material containing empty holes. It is the slice of an axially symmetric 3D object by a plane containing the symmetry axis of that object. A rotation of the image of Figure 3.2 (a) around the z axis must be performed in order to recover the 3D-object. We then focus on the tomographic reconstruction of the interior of the object (Figure 3.2 (b)).

[4]Note that the Laplacian operator should not be confused with the operator A defined as the opposite of the Dirichlet Laplacian on $L^2(-a, a)$, of domain $D(A) = H^1_0(-a, a) \cap H^2(-a, a)$. For instance, for every $f \in H^s_0(-a, a)$ with $s \in (0, 1) \setminus \{1/2\}$ (and $f \in H^{1/2}_{00}(-a, a)$ for $s = 1/2$), one has $f \in D(A^{s/2})$ and thus $A^{s/2} f \in L^2(-a, a)$ by definition, whereas $(-\Delta)^s f \in L^2(\mathbb{R}^n)$ (where f is extended by 0 outside $(-a, a)$) is not even of compact support. Recall that functions of $H^s_0(U)$ can be extended by 0 to $H^s(\mathbb{R}^n)$ for every $s \geqslant 0$ such that $s \notin \mathbb{N} + 1/2$; for $s = 1/2$ for instance, functions of $H^{1/2}_{00}(U)$ can be extended by 0 to $H^{1/2}(\mathbb{R}^n)$.

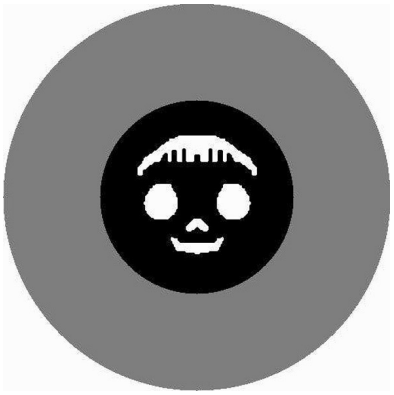

(a) Slice of a binary axially symmetric object by a plane containing the symmetry axis.

(b) Zoom on the interior of the object of Figure 3.2 (a); the homogeneous material is drawn in black and the holes in white.

Figure 3.2: Working example.

In our numerical simulations, we consider a Gaussian blur with standard deviation $\sigma_B = 0.12$, that is, modeled by a convolution with the kernel

$$K(x) = Ce^{-\frac{|x|^2}{2\sigma_B^2}} 1_{\tilde{\Omega}}(x),$$

where C is a normalizing constant so that $\int K d\mu = 1$. The noise is assumed to be a Gaussian noise τ with standard deviation $\sigma_\tau = 0.15$ (the image is rescaled between 0 and 1), that is,

$$\tau(x) = \frac{1}{\sqrt{2\pi}\sigma_\tau} e^{-\frac{|x|^2}{2\sigma_\tau^2}}.$$

We define the Signal to Noise Ratio as $SNR(v) = 20 \log_{10} \left(\|u_o\|_{L^2} / \|u_o - u_c\|_{L^2} \right)$, where u_o is the expected original image and u_c is the computed one. All numerical tests have been performed with the same data whose size was 256×256. For the noisy case (without blur) SNR= 2.66 and the SNR corresponding to the noisy and blurred data is 2.35 .

First, we have compared the methods of subsection 3.2 to compute ∇G_s. The most efficient is the use of the fractional laplacian. Indeed, the choice of Fourier transform leads to numerical instability together with bad reconstruction. This comes from the fact that the implementation of the FFT is not based on Bessel functions which are the natural special functions associated to the Radon transform. The use of exact formulas with Bessel functions gives better results but none was as good as the ones we obtained with the fractional laplacian.

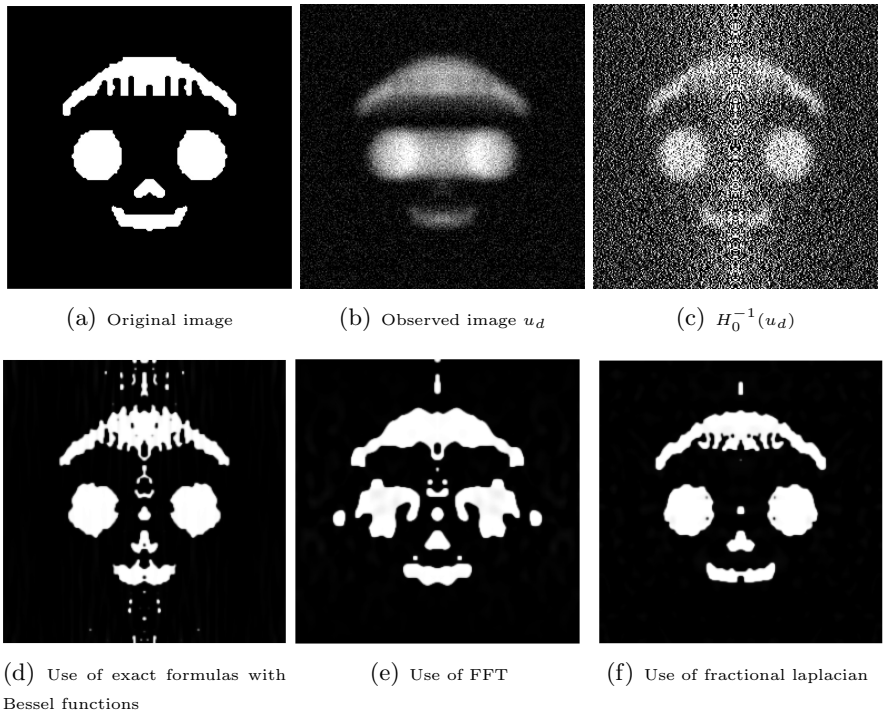

(a) Original image (b) Observed image u_d (c) $H_0^{-1}(u_d)$

(d) Use of exact formulas with Bessel functions (e) Use of FFT (f) Use of fractional laplacian

Figure 3.3: Results with Fourier approach : $s = 0.5, \varepsilon = 0.5, \alpha = 5, \beta = 0$

We have also tested the case where $\beta \neq 0$. If $\alpha = 0$ then the result is not satisfactory (see Figure 3.4). If $\alpha \neq 0$ the effect of β is null.

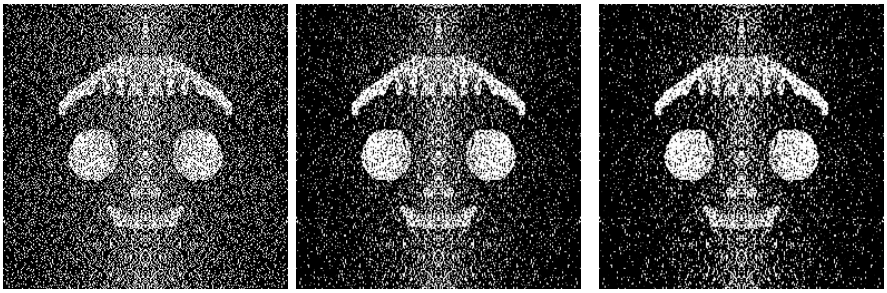

(a) $\alpha = 0,\ \beta = 10$ - SNR= -3.02 (b) $\alpha = 5,\ \beta = 10$ - SNR= -0.42 (c) $\alpha = 5,\ \beta = 5$ - SNR= 0.24

(d) $\alpha = 30,\ \beta = 0$- SNR= 9.62 (e) $\alpha = 30,\ \beta = 10$- SNR= 9.69 (f) $\alpha = 10,\ \beta = 0$- SNR= 5.54

Figure 3.4: Sensitivity with respect to β with $\varepsilon = 1e-02$ and $s = 0.5$ - no blur (Original SNR =2.66)

In the sequel, we focus on the case where $\beta = 0$ and ∇G_s is computed with the fractional Laplacian method of subesction 3.2.2.

3.3.1 Sensitivity to parameter s

In [1], similar numerical simulations were provided, corresponding to $s = 0$, that is, without any refined functional analysis of the Radon operator. For $s = 0$, the Radon operator H_0 is seen as a linear continuous operator from $L^2(\Omega)$ in $L^2(\Omega_1)$. Numerical simulations in this case are provided on Figure 3.5.

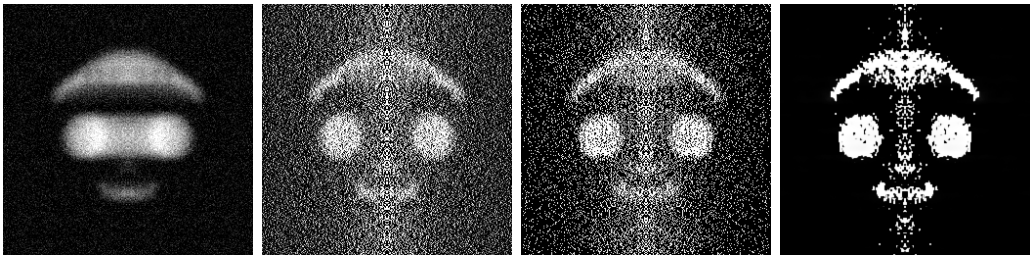

(a) Observed image u_d - SNR=2.35 (b) $H_0^{-1}(u_d)$ - SNR=0.02 (c) $\varepsilon = 0.1$, $\alpha = 1$ - SNR=-2.23 (d) $\varepsilon = 0.1$, $\alpha = 10$ - SNR=4.23

(e) $\varepsilon = 0.5$, $\alpha = 1$ - SNR=3.16 (f) $\varepsilon = 0.5$, $\alpha = 5$ - SNR=7.19 (g) $\varepsilon = 0.5$, $\alpha = 10$ - SNR=7.86 (h) $\varepsilon = 0.5$, $\alpha = 30$ - SNR=8.39

(i) $\varepsilon = 0.1$, $\alpha = 10$ - SNR=4.23 (j) $\varepsilon = 0.5$, $\alpha = 10$ - SNR=7.86 (k) $\varepsilon = 1$, $\alpha = 10$ - SNR= 8.35 (l) $\varepsilon = 1$, $\alpha = 5$ - SNR=8.03

Figure 3.5: Blur and noise (SNR = 2.35) - $s = 0$ (L^2 norm), simulations with different values of ε and α

r

As expected, and as already noted in [1], the quality of the reconstruction strongly depends on the specific choice of the parameters ε and α. Recall that α is the weight of the total variation. As expected, if α is too large, then the resulting image is too smooth, and if α is too small, then the image remains too much noisy. The penalization parameter ε is associated with the binarity constraint. If ε is too large then the binary features of the object are not well recovered and details are too much smoothened.

We next provide numerical simulations with $0 < s < 1$. This is indeed the main contribution of [3] to state that the Radon transform enjoys strong regularity properties in fractional-order Hilbert spaces. As can be seen on next Figures, the benefit of considering such a Hilbert space is spectacular. The reconstruction is of high quality, and moreover the

algorithm is time-efficient. The reconstruction of Figure 3.6 is obtained with MATLAB and 100 iterations.

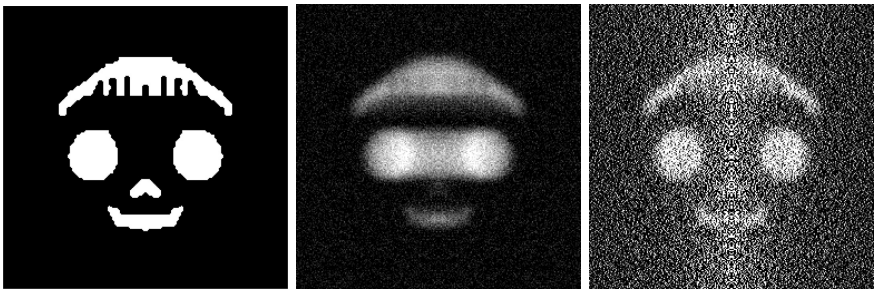

(a) Original image (b) Observed image u_d (c) $H_0^{-1}(u_d)$

(d) $s = 0$ - SNR = 7.86 (e) $s = 0.5$ - SNR = 8.04 (f) $s = 0.8$ - SNR = 7.58

Figure 3.6: Reconstruction with (H^s norm), for $\varepsilon = 0.5,\ \alpha = 10,\ \beta = 0$, nmax = 200 - Blur and noise

s	$F_{s,\alpha,\beta}$ (original)	$F_{s,\alpha,\beta}$ (computed)	$\|u_{orig} - u_{computed}\|$	SNR	CPU time (s)
0	2.082654e-01	2.257670e-01	2.716e-01	7.86	499
0.5	2.082654e-01	2.416019e-01	2.710e-01	8.04	433
0.8	2.082654e-01	2.466059e-01	2.902e-01	7.58	708

Table 1: Reconstruction with (H^s norm), for $\varepsilon = 0.5,\ \alpha = 10,\ \beta = 0$, nmax= 200 - Blur and noise

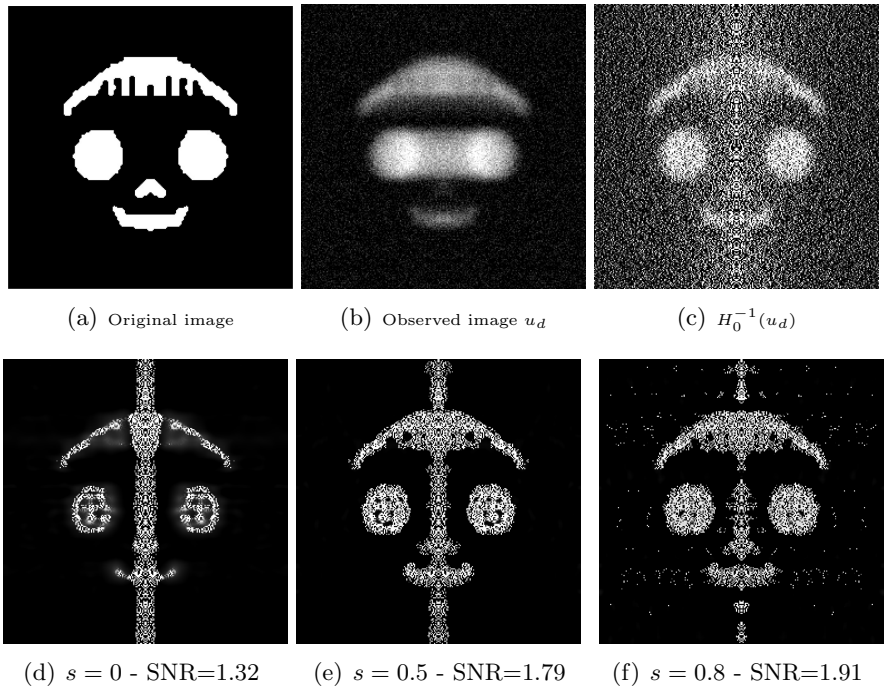

(a) Original image (b) Observed image u_d (c) $H_0^{-1}(u_d)$

(d) $s = 0$ - SNR=1.32 (e) $s = 0.5$ - SNR=1.79 (f) $s = 0.8$ - SNR=1.91

Figure 3.7: Reconstruction with (H^s norm), for $\varepsilon = 0.5$ without any additional penalization :$\alpha = 0$, $\beta = 0$, nmax =200 - Blur and noise

Other choices of the value of s, for instance $s = 0.75$, lead to similar results. The most spectacular improvement is obtained by considering a nonzero value of s (however required to be lower than 1). Note that, when s is chosen to be too close to 1, the reconstruction is too much smooth, as expected since the norm under consideration is close to the norm of H^1, which is not allowed in the continuous context.

3.3.2 Sensitivity with respect to the data

We have done several tests using different data.

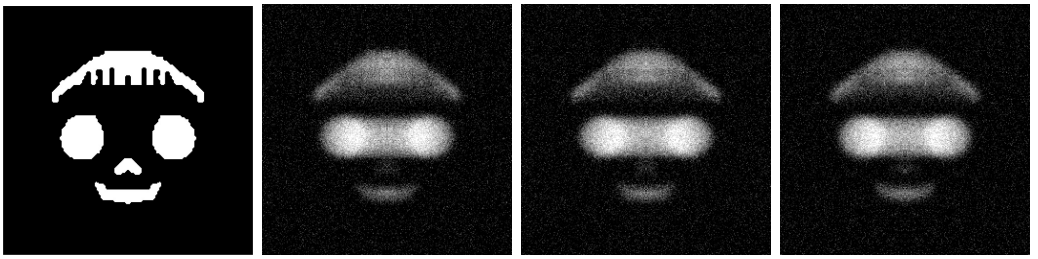

(a) Original image (b) Observed image 1 (c) Observed image 2 (d) Observed image 2

(e) Mean result for 50 different data - SNR = 11.68 (f) Result 1 - SNR = 9.96 (g) Result 2 - SNR = 9.80 (h) Result 3 - SNR = 9.27

Figure 3.8: Reconstruction for $s = 0.5, \varepsilon = 0.5, \alpha = 10,\ \beta = 0$, nmax=200 and different data. The left result is the mean image over 50 computations with 50 different data.

Remark 2. It was already noticed in [1] that the functional strongly decreases within small time and then decreases far more slowly. Actually, the image is considerably improved only after few iterations, far from the symmetry axis. This is due to the fact that the outermost pixels of the image carry more information than the innermost pixels. Indeed, since the object is axially symmetric, an outer pixel generates, when rotating around the symmetry axis z, a torus, which projects onto a strip on a plane containing the axis z. This strip is longer for an outer pixel than for an inner one, thus carrying more weight in the functional to be minimized in the iteration process. This is the reason why the convergence is slow for pixels around the axis, but very fast for outermost pixels.

We end this section reporting on CPU time with respect to the size of the quoted image. Computation avec been done with MATLAB software, so they are slow.

N	64	128	256	512	1024
CPU (s)	45.7	138.4	476.6	1172	3742
Normalized CPU	1	3	10.4	25.6	82

Table 2: CPU time sith respect to the image size $N \times N$, for $s = 0.5,\ \varepsilon = 0.5,\ \alpha = 10,\ \beta = 0$, nmax= 200 - Blur and noise

We note that the process is not very fast. Therefore we use a wavelet approach that is described in next section.

4 A needlet approach

In this section, we describe an approach of smoothed Fourier series type based on a SVD type decomposition of the Radon projection operator H_0.

4.1 Abel integral and Jacobi based inversion formula

Let us start by observing that the Radon projection operator H_0 defined by (1.1) is related to the classical Abel integral transform $T_{1/2}u(x) = \int_0^x \frac{u(t)}{(x-t)^{1/2}}\,dt$ by the relation

$$H_0u(y,z) = \int_0^{1-|y|^2} u(\sqrt{1-t},z)\frac{1}{\sqrt{1-y^2-t}}\,dt = T_{1/2}\overline{u}_z(1-y^2),$$

where $\overline{u}_z(t) = u(\sqrt{1-t},z)$, for every $u \in BV(\Omega)$.

For all $(\alpha,\beta) \in (-1,+\infty)^2$ and every $m \in \mathbb{N}$, let $J^{\alpha,\beta}_{[-1,1],m}$ denote the n-th degree Jacobi polynomial defined on $[-1,1]$, and let

$$J^{\alpha,\beta}_m(x) = \sqrt{\frac{n!(2n+\alpha+\beta+1)\Gamma(n+\alpha+\beta+1)}{\Gamma(n+\alpha+1)\Gamma(n+\beta+1)}}J^{\alpha,\beta}_{[-1,1],m}(2x-1),$$

for every $x \in [0,1]$. The family $(J^{\alpha,\beta}_n)_{m\in\mathbb{N}}$ is an Hilbertian basis of the (weighted) Hilbert space $L^2([0,1],(1-x)^\alpha x^\beta dx)$. In [**?**], the authors provide a SVD type decomposition of the operator $T_{1/2}$, showing in particular that

$$T_{1/2}(J^{0,0}_m)(x) = \beta_m x^\alpha J^{-1/2,1/2}_m(x),$$

for every $m \in \mathbb{N}$ and for every $x \in [0,1]$, where

$$\beta_m = \Gamma(1/2)\sqrt{\frac{\Gamma(m+1/2)}{\Gamma(m+3/2)}} \sim \frac{\Gamma(1/2)}{(m+3/2)^{1/2}}.$$

In terms of the Radon operator H_0, it follows that

$$H_0\left(J^{0,0}_m(1-r^2)g(z)\right)(y,z) = \beta_m\sqrt{1-y^2}J^{-1/2,1/2}_m(1-y^2)g(z)$$

for every function $g \in L^2(-1,1)$.

Let $Q_n(r) = J^{(0,0)}_m(1-r^2)$ and $Q^{\#}_m(y) = J^{(-1/2,1/2)}_m(1-y^2)$, by construction, $(Q_m)_{m\in\mathbb{N}}$ and $(Q^{\#}_m)_{m\in\mathbb{N}}$ are orthonormal bases of respectively $L^2(0,1,2rdr)$ and $L^2(0,1,2\sqrt{1-y^2}dy)$. Therefore any $u \in L^2(\Omega,2rdrdz)$ can be expanded along r as

$$u(r,z) = \sum_{m\in\mathbb{N}}\left(\int_0^1 u(r',z)Q_m(r')2r'dr'\right)Q_m(r')$$

and thus

$$H_0u(y,z) = \sum_{m\in\mathbb{N}} \left(\int_0^1 u(r',z) Q_m(r') 2r' dr' \right) \beta_m \sqrt{1-y^2} Q_m^{\#}(y)$$
$$= \sum_{m\in\mathbb{N}} \left(\int_0^1 H_0u(y',z) Q_m^{\#}(y') 2dy' \right) Q_m(r') \sqrt{1-y^2} Q_m^{\#}(y).$$

We derive thus the following one-dimensional inversion formula:

Lemma 2. *For every $u \in L^2(\Omega, 2rdrdz)$,*

$$u(r,z) = \sum_{m=0}^{+\infty} \frac{1}{\beta_m} \left(\int_0^1 (H_0u)(y',z) Q_m^{\#}(y') 2\, dy' \right) Q_m(r). \tag{4.1}$$

For any orthonormal basis of $L^2(-1,1)$ $(R_m)_{m\in\mathbb{N}}$, this formula yields a two-dimensional inversion formula:

Lemma 3. *For every $u \in L^2(\Omega, 2rdrdz)$,*

$$u(r,z) = \sum_{m=0}^{+\infty} \sum_{m'=0}^{+\infty} \frac{1}{\beta_m} \left(\int_{-1}^1 \int_0^1 (H_0u)(y',z') Q_m^{\#}(y') R_{m'}(z') 2\, dy' dz' \right) Q_m(r) R_{m'}(z). \tag{4.2}$$

Although the previous formula is valid for any orthogonal basis $(R_m)_{m\in\mathbb{N}}$, we will use in the following the choice $R_m = J_m^{(0,0)}$, i.e. the Legendre polynomial basis. This choice may seem arbitrary and unnecessarily complex. It turns out that the Legendre polynomial basis is nevertheless the simplest orthogonal basis of $L^2(-1,1)$ considered as an interval without any periodization. This polynomial basis has also, for any degree, some explicit cubature formula, a property which will proved to be important later on. A construction similar to the one proposed below could also be made with a Fourier basis but it suffers from periodization artifacts that are avoided by the choice of the Legendre polynomial basis.

4.2 Smoothed inversion and needlets

Assume now, as it is the case in practice, that we have only access to some approximations $\widetilde{h_{m,m'}}$ of

$$h_{m,m'} = \int_{-1}^1 \int_0^1 (H_0u)(y',z') Q_m^{\#}(y') R_{m'}(z') 2\, dy' dz'$$

for $0 \leqslant m \leqslant M$ and $0 \leqslant m' \leqslant M'$, how to use the previous formula to reconstruc an estimate of the function u?

Hard truncation, and Gibbs phenomenon. The most natural answer is to use the truncated reconstruction

$$\widetilde{P_{M,M'}u} = \sum_{m=0}^{M}\sum_{m'=0}^{M'} \frac{\widetilde{h_{m,m'}}}{\beta_m} Q_m(r')R_{m'}(z). \tag{4.3}$$

Although optimal from the quadratic risk point of view, this reconstruction however suffers from well known Gibbs type artifacts. Gibbs phenomena are well known in inverse problems and here in our tomography problem they appear to be so strong that they make the use of such an inversion formula not suitable in the problem.

Smoothened truncation. As examplified in [5] in the Fourier case and in [13] for Jacobi polynomials, there exists a simple method in order to cancel the Gibbs phenomenon. Let us recall this approach and show how it can be adapted and used in our context in a relevant way.

Let a be an arbitrary smooth nonnegative function supported in $[0,1]$, such that $a(w) = 1$ for every $w \in [0,1/2]$ and $a(w) \leqslant 1$ for every $w \in (1/2,1]$. The method consists of replacing the hard truncation (4.3) with a soft one, by considering

$$\widetilde{P_{M,M'}u}(r) = \sum_{m=0}^{+\infty}\sum_{m'=0}^{+\infty} a\left(\frac{m}{M}\right) a\left(\frac{m'}{M'}\right) \frac{\widetilde{h_{m,m'}}}{\beta_m} Q_m(r)R_{m'}(z). \tag{4.4}$$

Note that the hard truncation would correspond to $a(w) = \chi_{[0,1]}(w)$. In Fourier series, the Fejer kernel corresponds to the choice $a(w) = \max(1-w,0)$ and is known to leads to better approximation. One can understand this smoothing effect through the study of the corresponding smoothed projector

$$P_{a,M,M'}u = \sum_{m=0}^{M}\sum_{m'=0}^{M} a\left(\frac{m}{M}\right) a\left(\frac{m'}{M'}\right) c_{m,m'}Q_m(r)R_{m'}(z).$$

with

$$c_{m,m'} = \int_0^1 u(r',z')Q_m(r')R_{m'}(z')2r'\,dr'dz'$$

Indeed, as soon as a is smooth, say $\mathcal{C}^\infty$, then those projectors satisfy some very nice properties, for instance all projections are now continuous for all L^p norms.

The best insight on those smoothened projection is probably the one proposed in [13]. Following their approach, the projection is first rewritten as a convolution

$$P_{a,M,M'}u = \int_{-1}^1 u(r',z')A_{a,M,M'}(r,z,r',z')2r'dr'dz'$$

with a kernel $A_{a,M,M'}$

$$A_{a,M,M'}(r,z,r',z') = \sum_{m=0}^{M}\sum_{m'=0}^{M'} a\left(\frac{m}{M}\right) a\left(\frac{m'}{M'}\right) Q_m(r)R_{m'}(z)Q_m(r')R_{m'}(z').$$

One of the main result of this paper is to prove that if $a \in \mathcal{C}^\infty$ then this kernel is well localized spatially: for all $k \in \mathbb{N}, \exists c_k > 0$ such that

$$|A_{a,M,M'}(r,z,r',z')| \leqslant \frac{c_K M M'}{(1+Md(1-2r^2,1-2r'^2))^K (1+M'd(z,z'))^K \gamma(M,M',r,z,r',z')}$$

where $d(u,v) = |\arccos(u,v)|$ and

$$\gamma(M,M',r,z,r',z') = \sqrt{w_{0,0}(M,1-2r^2)w_{0,0}(M,1-2r'^2)w_{0,0}(M',z)w_{0,0}(M',z')}$$

with $w_{\alpha,\beta}(M,u) = (u+M^{-2})^{\alpha+1/2}(u-1+N^{-2})^{\beta+1/2}$. This result is sufficient to obtain the L^p continuity of the projection. Furthermore, one verify the existence of $c > 1$ such that

$$\int_{-1}^{1}\int_{0}^{1} \left|P_{a,M,M'}u(r,z) - u(r,z)\right|^p 2rdrdz \leqslant c \inf_{v \in \mathrm{Span}\{Q_m(1-r^2)R_{m'}(z)\}_{0\leqslant m\leqslant M/2, 0\leqslant m'\leqslant M'/2}} \int_{-1}^{1}\int_{0}^{1} |v(r,z)-u(r,z)|^p 2rdrdz$$

It turns out that this projection can be *discretized* as soon as there is a quadrature formula polynomials of finite degrees. Indeed, let Ξ_j be a set of quadrature point such that for any $Q_n(r)R_{n'}(z)$ and $Q_m(r)R_{m'}(z)$ with n, n', m and m' smaller than 2^j

$$\int_{-1}^{1}\int_{0}^{1} Q_n(r)R_{n'}(z)Q_m(r)R_{m'}(z)2rdrdz = \sum_{\xi=(r_\xi,z_\xi)\in\Xi_{2^j}} \omega_\xi Q_n(r_\xi)R_{n'}(z_\xi)Q_m(r_\xi)R_{m'}(z_\xi),$$

and define

$$\phi^{a,a}_{j,\xi}(r,z) = \sqrt{\omega_\xi} \sum_{m\in\mathbb{N}}\sum_{m'\in\mathbb{N}} \sqrt{a\left(\frac{m}{2^j}\right) a\left(\frac{m'}{2^j}\right)} Q_m(r_\xi)R_{m'}(z_\xi)Q_m(r)R_{m'}(z)$$

then

$$P_{a,2^j,2^j}u(r,z) = \sum_{\xi\in\Xi_j} d^{a,a}_{j,\xi}\phi^{a,a}_{j,\xi}(r,z)$$

with

$$d^{a,a}_{j,\xi} = \int_{-1}^{1}\int_{0}^{1} u(r',z')\phi^{a,a}_{j,\xi}(r',z')2r'dr'dz'.$$

Finally, if the quadrature points are chosen as the zeros of $Q_{2^{j+1}}(1-r^2)R_{2^{j+1}}(z)$ then forall $k \in \mathbb{N}, \exists c'_k$ such that

$$|\phi^{a,a}_{j,\xi}(r,z)| \leqslant \frac{c'_K 2^j}{(1+2^j d(1-2r^2,1-2r_\xi^2))^K (1+2^j d(z,z_\xi))^K \gamma(2^j,2^j,r,z,r_\xi,z_\xi)}.$$

Furthermore, $\forall p \in [1,+\infty], \exists (c_p, C_p, D_p) \in \mathbb{R}^3_{+,*}$ such that

$$\forall j \in \mathbb{N}, \forall \xi \in \Xi_j, c_p 2^{j(p/2-1)} \leqslant \int_{-1}^{1}\int_{0}^{1} |\phi^{a,a}_{j,\xi}(r,z)|^p 2rdrdz \leqslant C_p 2^{j(p/2-1)}$$

$$\forall d^{a,a}_{j,\xi} \in \mathbb{R}^{\Xi_j}, \int_{-1}^{1}\int_{0}^{1} |\sum_{\xi\in\Xi_j} d^{a,a}_{j,\xi}\phi^{a,a}_{j,\xi}(r,z)|^p 2rdrdz \leqslant C_p D_p 2^{j(p/2-1)} \sum_{\xi\in\Xi_j} |d^{a,a}_{j,\xi}|^p.$$

Needlets. The needlets corresponds to a multiscale representation associated to those projection. More precisely, for any $J > 0$

$$P_{a,2^J,2^J} = P_{a,1,1} + \sum_{j=1}^{J} \left(P_{a,2^j,2^j} - P_{a,2^{j-1},2^{j-1}}\right)$$

where by construction

$$P_{a,2^j,2^j} - P_{a,2^{j-1},2^{j-1}} u = \int_{-1}^{1} u(r',z') B_{a,2^j,2^j}(r,z,r',z') 2r'dr'dz'$$

with

$$B_{a,2^j,2^j}(r,z,r',z') = \sum_{m=0}^{2^j}\sum_{m'=0}^{2^j} \left(a\left(\frac{m}{2^j}\right) a\left(\frac{m'}{2^j}\right) - a\left(\frac{m}{2^{j-1}}\right) a\left(\frac{m'}{2^{j-1}}\right)\right) Q_m(r)R_{m'}(z)Q_m(r')R_{m'}(z').$$

So that if we let $b(w) = a(w) - a(2w)$ and use $a(w)a(w') = a(2w)a(2w') + a(w)b(w') + b(w)a(w') + b(w')b(w')$

$$\begin{aligned} B_{a,2^j,2^j}(r,z,r',z') = &\sum_{m=0}^{2^j}\sum_{m'=0}^{2^j} a\left(\frac{m}{2^j}\right) b\left(\frac{m'}{2^j}\right) Q_m(r)R_{m'}(z)Q_m(r')R_{m'}(z') \\ &+ \sum_{m=0}^{2^j}\sum_{m'=0}^{2^j} b\left(\frac{m}{2^j}\right) a\left(\frac{m'}{2^j}\right) Q_m(r)R_{m'}(z)Q_m(r')R_{m'}(z') \\ &+ \sum_{m=0}^{2^j}\sum_{m'=0}^{2^j} b\left(\frac{m}{2^j}\right) b\left(\frac{m'}{2^j}\right) Q_m(r)R_{m'}(z)Q_m(r')R_{m'}(z'). \end{aligned}$$

Using the cubature Ξ_j and defining the needlets

$$\psi^{b,a}_{j,\xi}(r,z) = \sqrt{\omega_\xi} \sum_{m\in\mathbb{N}}\sum_{m'\in\mathbb{N}} \sqrt{b\left(\frac{m}{2^j}\right) a\left(\frac{m'}{2^j}\right)} Q_m(r_\xi)R_{m'}(z_\xi)Q_m(r)R_{m'}(z)$$

$$\psi^{a,b}_{j,\xi}(r,z) = \sqrt{\omega_\xi} \sum_{m\in\mathbb{N}}\sum_{m'\in\mathbb{N}} \sqrt{a\left(\frac{m}{2^j}\right) b\left(\frac{m'}{2^j}\right)} Q_m(r_\xi)R_{m'}(z_\xi)Q_m(r)R_{m'}(z)$$

$$\psi^{b,b}_{j,\xi}(r,z) = \sqrt{\omega_\xi} \sum_{m\in\mathbb{N}}\sum_{m'\in\mathbb{B}} \sqrt{b\left(\frac{m}{2^j}\right) b\left(\frac{m'}{2^j}\right)} Q_m(r_\xi)R_{m'}(z_\xi)Q_m(r)R_{m'}(z),$$

one obtains

$$\left(P_{a,2^J,2^J} - P_{a,2^{J-1},2^{J-1}}\right) u = \sum_{o\in\{(a,b),(b,a),(b,b)} \sum_{\xi\in\Xi_J} d^o_{j,\xi})\psi^o_{J,\xi}$$

with

$$d^o_{j,\xi} \int_{-1}^{1}\int_{0}^{1} u(r',z')\psi^o_{j,\xi}(r',z')2r'dr'dz'.$$

Summing those equality over J yields

$$P_{a,2^J,2^J} u = \sum_{\xi\in\Xi_0} a_{j,\xi}\phi^{a,a}_{0,\xi} + \sum_{o\in\{(a,b),(b,a),(b,b)} \sum_{j=0}^{J}\sum_{\xi\in\Xi_j} d^o_{j,\xi}\psi^{a,b}_{j,\xi}$$

which implies that

$$\left\{\phi^{a,a}_{1,\xi}\right\}_{\xi\in\Xi_0} \cup \bigcup_{j\geqslant 0} \bigcup_{o\in\{(a,b),(b,a),(b,b)\}} \left\{\psi^o_{2^j,\xi}\right\}_{\xi\in\Xi_j}$$

is a tight frame.

Again, if the quadrature points are chosen as the zeros of $Q_{2^{j+1}}(1-r^2)R_{2^{j+1}}(z)$ then forall $k\in\mathbb{N}, \exists c'_k$ such that

$$|\psi^o_{j,\xi}(r,z)| \leqslant \frac{c'_K 2^j}{(1+2^j d(1-2r^2,1-2r^2_\xi))^K (1+2^j d(z,z_\xi))^K \gamma(2^j,2^j,r,z,r_\xi,z_\xi)}.$$

Furthermore, $\forall p\in[1,+\infty], \exists (c_p,C_p,D_p)\in\mathbb{R}^3_{+,*}$ such that

$$\forall j\in\mathbb{N}, \forall\xi\in\Xi_j, c_p 2^{j(p/2-1)} \leqslant \int_{-1}^{1}\int_{0}^{1} |\psi^o_{j,\xi}(r,z)|^p 2rdrdz \leqslant C_p 2^{j(p/2-1)}$$

$$\forall d^o_{j,\xi}\in\mathbb{R}^{3\times\Xi_j}, \int_{-1}^{1}\int_{0}^{1} |\sum_o\sum_{\xi\in\Xi_j} d^o_{j,\xi}\psi^o_{j,\xi}(r,z)|^p 2rdrdz \leqslant C_p D_p 2^{j(p/2-1)} \sum_o\sum_{\xi\in\Xi_j} |d^o_{j,\xi}|^p.$$

This implies that the L^p norm of u can be controlled through the needlet coefficients and thus that it suffices to well estimate the needlet coefficients to well estimate the function as shown in the companion paper.

Needlet coefficient estimation. To produce a good estimate of u, it suffices thus to produce good estimates for the needlet coefficients:

$$\int_{-1}^{1}\int_{0}^{1} u(r',z')\psi^o_{j,\xi}(r',z')2r'dr'dz'.$$

Using the definition, one has for $\psi^o_{j,\xi}$:

$$\begin{aligned}
d^o_{j,\xi} &= \int_{-1}^1 \int_0^1 u(r,z)\psi^o_{j,\xi}(r,z)2rdrdz \\
&= \int_{-1}^1 \int_0^1 u(r,z)\left(\sqrt{\omega_\xi}\sum_{m\in\mathbb{N}}\sum_{m'\in\mathbb{N}}\sqrt{o_1\left(\frac{m}{2^j}\right)o_2\left(\frac{m'}{2^j}\right)}Q_m(r_\xi)R_{m'}(z_\xi)Q_m(r)R^{(0,0)}_{m'}(z)\right)2rdrdz' \\
&= \sqrt{\omega_\xi}\sum_{m\in\mathbb{N}}\sum_{m'\in\mathbb{N}}\sqrt{o_1\left(\frac{m}{2^j}\right)o_2\left(\frac{m'}{2^j}\right)}Q_m(r_\xi)R_{m'}(z_\xi)\left(\int_{-1}^1\int_0^1 u(r,z)Q_m(r)R_{m'}(z)2rdrdz\right) \\
&= \sqrt{\omega_\xi}\sum_{m\in\mathbb{N}}\sum_{m'\in\mathbb{N}}\sqrt{o_1\left(\frac{m}{2^j}\right)o_2\left(\frac{m'}{2^j}\right)}Q_m(r_\xi)R_{m'}(z_\xi)\frac{h_{m,m'}}{\beta_m}.
\end{aligned}$$

A natural estimate for $d^o_{j,\xi}$ is thus given by

$$\widetilde{d^o_{j,\xi}} = \sqrt{\omega_\xi}\sum_{m\in\mathbb{N}}\sum_{m'\in\mathbb{N}}\sqrt{o_1\left(\frac{m}{2^j}\right)o_2\left(\frac{m'}{2^j}\right)}Q_m(r_\xi)R_{m'}(z_\xi)\frac{\widetilde{h_{m,m'}}}{\beta_m}.$$

Note that by construction

$$\begin{aligned}
\widetilde{P_{a,2^J,2^J}u} = \sum_{\xi\in\Xi_0}\widetilde{d^{a,a}_{0,\xi}}\phi^{a,a}_{0,\xi} + \sum_{j=0}^J\sum_o\sum_{\xi\in\Xi_j}\widetilde{d^o_{j,\xi}}\psi^0_{j,xi} \\
= \sum_{n=0}^{2^J}\sum_{n'=0}^{2^J} a\left(\frac{n}{2^J}\right)a\left(\frac{n'}{2^J}\right)\frac{\widetilde{h_{n,n'}}}{\beta_n}Q_n(r)R_{n'}(z)
\end{aligned}$$

and thus the needlets seem not to be useful as the second formula is simpler.

It turns out that this estimate can be transformed in a better one in terms of expected error by thresholding the estimated coefficients, i.e. replacing them by 0 when they are small. This idea has been introduced by Donoho et al in statistics and relies on apprimation theory. It is based on the observation that if a needlet coefficient $d^o_{j,\xi}$ of the true function u is small with respect to the approximation error between $d^o_{j,\xi}$ and $\widetilde{d^o_{j,\xi}}$ then it is better to replace the approximated value by 0. This idea can not be used as is as the value of $d^o_{j,\xi}$ is unknow but it is replaced by a decision based on a comparison between the approximation $\widetilde{d^o_{j,\xi}}$ and a threshold $T_{j,\xi}$ meant as an expected error term. This yields the thresholding estimate

$$\widetilde{u}_J = \sum_{\xi\in\Xi_0}\widetilde{d^{a,a}_{0,\xi}}\phi^{a,a}_{0,\xi} + \sum_{j=0}^J\sum_o\sum_{\xi\in\Xi_j}\rho_{T_{j,\xi}}\left(\widetilde{d^o_{j,\xi}}\right)\psi^0_{j,xi}$$

with $\rho_T(x) = x$ if $|x| > T$ and 0 otherwise and $T_{j,\xi}$ is a family of threshold to be chosen. For instance, in a Gaussian white noise framework, $T_{j,\xi}$ is chosen as a multiple of the expected standard deviation.

As soon as there is some blurring, the inversion formula (4.2) does not hold anymore. Following ideas of [**?**], we propose to simply apply a regularized inverse operator B_ρ^{-1} to the noisy observation $v_d = BH_O u + \tau$ and apply the thresholded needlet estimator to $B_\rho^{-1} v_d$. The choice of the thresholds should be modified according to the specific inverse used. This issue is discussed below.

Algorithm 2

Compute $I_d = B_\rho^{-1} v_d$

For $0 \leqslant n, n' \leqslant 2^J$, compute $h_{n,n'} = \dfrac{8}{2^{2J}} \displaystyle\sum_{i=1}^{N/2} \sum_{j=1}^{N} I_d[i,j] Q_n^{\#}(2i/N) R_{n'}(i/N - 1)$

For $\xi \in \Xi_0$, compute $d_{0,\xi}^{a,a} = \dfrac{h_{0,0}}{\beta_0} Q_0(r_\xi) R_0(z_\xi)$

For $0 \leqslant j \leqslant J$, for $\xi \in \Xi_j$, for all o, compute

$$\widetilde{d_{j,\xi}^{o}} = \sqrt{\omega_\xi} \sum_{n=0}^{2^j} \sum_{n'=0}^{2^j} \sqrt{o_1\left(\frac{n}{2^j}\right) o_2\left(\frac{n'}{2^j}\right)} Q_n(r_\xi) R_{n'}(z_\xi) \frac{\widetilde{h_{n,n'}}}{\beta_n}$$

and $\rho_{T_{j,\xi}}(\widetilde{d_{j,\xi}^{o}})$

Set

$$\widetilde{u}^{Th} = \sum_{\xi \in \Xi_0} \widetilde{d_{0,\xi}^{a,a}} \phi_{0,\xi}^{a,a} + \sum_{j=0}^{J} \sum_{o} \sum_{\xi \in \Xi_j} \rho_{T_{j,\xi}}\left(\widetilde{d_{j,\xi}^{o}}\right) \psi_{j,xi}^{0}$$

where $v_d[i,j] = v_d(2i/N, i/N - 1)$.

5 Conclusion

In this article we have designed two different numerical approaches in order to solve the tomographic reconstruction problem (1.2), where the unknown density function is binary, axially symmetric, and the observed data are strongly blurred and noised.

Our first approach is variational and consists of minimizing a penalized functional defined in some fractional order Hilbert spaces that are defined according to the regularity properties of the Radon transform. We have developed an algorithm solving the first-order optimality system by a Newton-like procedure, and the gradient of the fractional Hilbert norm is computed using a fractional Laplacian.

Our second approach consists of designing a needlet-based inversion formula for reconstructing the density, based on properties of the Radon transform in Jacobi polynomial basis and on smoothing considerations in order to avoid Gibbs phenomena.

References

[1] R. Abraham, M. Bergounioux, E. Trélat, *A penalization approach for tomographic reconstruction of binary radially symmetric objects*, Applied Mathematics and Optimization **58** (2008), no. 3, 345–371.

[2] G. Ambartsoumian, P. Kuchment, *A range description for the planar circular Radon transform*, SIAM J. Math. Anal. **38** (2006), no. 2, 681–692.

[3] M. Bergounioux, E. Trélat, *A variational method using fractional order Hilbert spaces for tomographic reconstruction of blurred and noised binary images*, J. Funct. Anal. **259** (2010), no. 9, 2296–2332.

[4] A. Chambolle, *An algorithm for total variation minimization and applications*, Journal of Mathematical Imaging and Vision **20**, 1-2 (2004), 89–97.

[5] D. Gottlieb, C.-W. Shu, *On the Gibbs phenomenon and its resolution*, SIAM Rev. **39** (1997), no. 4, 644–668.

[6] M. Greenblatt, *A method for proving L^p boundedness of singular Radon transforms in codimension one for* $1 < p < \infty$, Duke Math. J. **108** (2001), no. 2, 363–393.

[7] S. Helgason, *The Radon Transform*, Birkhäuser, Basel, 1980.

[8] S. Helgason, *Ranges of Radon transforms*, Computed tomography (Cincinnati, Ohio, 1982), pp. 63–70, Proc. Sympos. Appl. Math., 27, Amer. Math. Soc., Providence, R.I., 1982.

[9] A. Hertle, *On the range of the Radon transform and its dual*, Math. Ann. **267** (1984), no. 1, 91–99.

[10] B .Hofmann, B. Kaltenbacher, C. Pöschl, O. Scherzer, *A convergence rates result for Tikhonov regularization in Banach spaces with non-smooth operators*, Inverse Problems **23** (2007) 9871010

[11] F. Natterer, *Exploiting the ranges of Radon transforms in tomography*, Numerical treatment of inverse problems in differential and integral equations (Heidelberg, 1982), 290–303, Progr. Sci. Comput., 2, Birkhäuser, Boston, Mass., 1983.

[12] Y. Nesterov, *Smooth minimization of non-smooth functions.* Mathematic Programming, Ser. A 103, 127–15 .2005.

[13] P. Petrushev, Y. Xu, *Localized polynomial frames on the interval with Jacobi weights*, J. Fourier Anal. Appl. **11** (2005), no. 5, 557–575.

[14] P. Weiss, L. Blanc-Féraud, G. Aubert, *Efficient schemes for total variation minimization under constraints in image processing*, SIAM J. Sci. Comput., 31(3), 2047-2080.